

See discussions, stats, and author profiles for this publication at: <https://www.researchgate.net/publication/235878894>

Mechanistic Characterization of the Tetraacyldisaccharide-1-phosphate 4'-Kinase LpxK Involved in Lipid A Biosynthesis

ARTICLE *in* BIOCHEMISTRY · MARCH 2013

Impact Factor: 3.02 · DOI: 10.1021/bi400097z · Source: PubMed

CITATIONS

3

READS

39

5 AUTHORS, INCLUDING:



Ryan P Emptage

University of Pennsylvania

3 PUBLICATIONS 9 CITATIONS

[SEE PROFILE](#)



Pei Zhou

Duke University Medical Center

86 PUBLICATIONS 2,542 CITATIONS

[SEE PROFILE](#)

Mechanistic Characterization of the Tetraacyldisaccharide-1-phosphate 4'-Kinase LpxK Involved in Lipid A Biosynthesis

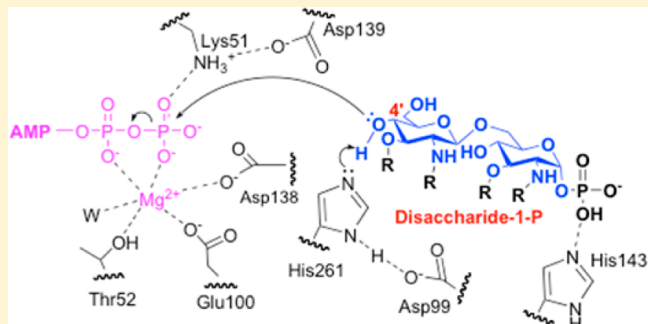
Ryan P. Emptage,*† Charles W. Pemble, IV,‡ John D. York,§ Christian R. H. Raetz,† and Pei Zhou*,†

†Department of Biochemistry and ‡Human Vaccine Institute, Duke University Medical Center, Durham, North Carolina 27710, United States

§Department of Biochemistry, Vanderbilt University School of Medicine, Nashville, Tennessee 37205, United States

Supporting Information

ABSTRACT: The sixth step in the lipid A biosynthetic pathway involves phosphorylation of the tetraacyldisaccharide-1-phosphate (DSMP) intermediate by the cytosol-facing inner membrane kinase LpxK, a member of the P-loop-containing nucleoside triphosphate (NTP) hydrolase superfamily. We report the kinetic characterization of LpxK from *Aquifex aeolicus* and the crystal structures of LpxK in complex with ATP in a precatalytic binding state, the ATP analogue AMP-PPC in the closed catalytically competent conformation, and a chloride anion revealing an inhibitory conformation of the nucleotide-binding P-loop. We demonstrate that LpxK activity in vitro requires the presence of a detergent micelle and formation of a ternary LpxK–ATP/Mg²⁺–DSMP complex. Using steady-state kinetics, we have identified crucial active site residues, leading to the proposal that the interaction of D99 with H261 acts to increase the pK_a of the imidazole moiety, which in turn serves as the catalytic base to deprotonate the 4'-hydroxyl of the DSMP substrate. The fact that an analogous mechanism has not yet been observed for other P-loop kinases highlights LpxK as a distinct member of the P-loop kinase family, a notion that is also reflected through its localization at the membrane, lipid substrate, and overall structure.



Gram-negative bacteria differentiate themselves from their Gram-positive counterparts by the presence of an outer membrane, the outer leaflet of which is composed of the lipid-anchored complex carbohydrate known as lipopolysaccharide (LPS). The lipid portion of LPS is an acylated glucosamine disaccharide known as lipid A, which even without the presence of the immunogenic O-antigen can elicit a mammalian inflammatory response through activation of the macrophage Toll-like receptor 4 and myeloid differentiation protein 2 complex (TLR4–MD2).^{1,2} Nine enzymatic steps make up the constitutive pathway of lipid A biosynthesis in *Escherichia coli*, and because lipid A is essential for the viability of the vast majority of Gram-negative bacteria, the pathway stands as an attractive target for the development of novel antimicrobials.³

The sixth step of the lipid A biosynthetic pathway is the phosphorylation of the 4'-hydroxyl group of tetraacyldisaccharide-1-phosphate (DSMP) as catalyzed by LpxK, a divergent member of the P-loop-containing nucleoside triphosphate (NTP) hydrolase superfamily (Pfam02606, CL0023), which resides on the cytosolic face of the inner membrane (Scheme 1).^{4–7} The active site Walker A (P-loop) and Walker B (Mg²⁺-binding) motifs are common to all P-loop kinase family members.⁸ Recent structural characterization of LpxK from *Aquifex aeolicus* revealed a two- $\alpha/\beta/\alpha$ domain topology in which the second $\alpha/\beta/\alpha$ domain, a substructure unique to LpxK, was implicated in nucleotide binding through a hinge

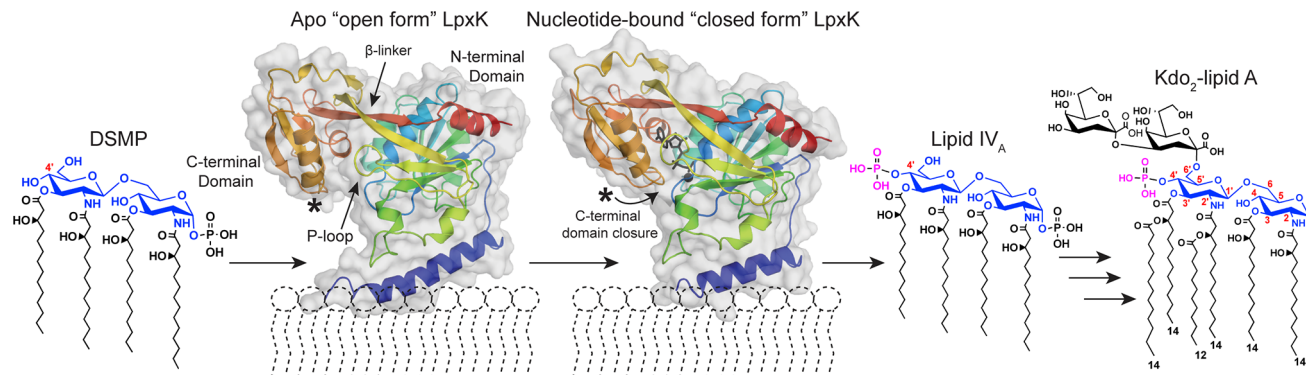
motion about its base (Scheme 1).⁹ Further analysis led to the conclusion that the hydrophobic lower face of the N-terminal helix may be responsible for membrane association, assisted by charge–charge interactions of surrounding basic residues with the anionic phospholipids of the membrane. Despite some differences with regard to the presence of N- versus O-linked acyl chains and chain lengths of *Aquifex* DSMP,^{10,11} *A. aeolicus* LpxK can readily phosphorylate the *E. coli*-derived DSMP substrate.⁹

A handful of P-loop kinases have been kinetically characterized; however, determination of a conserved catalytic mechanism has remained elusive, possibly because of the fact that P-loop kinases have evolved to act upon a highly diverse array of substrates.^{4,12} Structural and kinetic characterization of several P-loop kinases has suggested direct nucleophilic attack by the acceptor substrate, either assisted or unassisted by an aspartate/glutamate catalytic base of the Walker B motif.^{12–14} A distribution of positively charged residues in the active site, especially the conserved P-loop lysine, may assist in shielding the negative charges generated during phosphate transfer. For a few kinases and sulfotransferases outside of the P-loop kinase family, a histidine residue has been implicated as a general base

Received: January 25, 2013

Revised: March 5, 2013

Published: March 7, 2013

Scheme 1. Reaction Catalyzed by LpxK in Kdo₂-Lipid A Biosynthesis^a

^aLpxK is responsible for the phosphorylation (purple) of the 4'-hydroxyl of tetraacyldisaccharide-1-phosphate (DSMP). Positions on the glucosamine backbone (blue) of DSMP are labeled (red). The crystal structures of apo *A. aeolicus* LpxK (PDB entry 4EHX) and ADP/Mg²⁺-bound LpxK (PDB entry 4EHY) in their predicted membrane orientations are included and colored from N- to C-terminus (blue to red, respectively). ADP is shown as black sticks, and Mg²⁺ is shown as a black sphere in the "closed" form. The N-terminal helix (blue cartoon) is implicated in membrane binding through a hydrophobic lower face assisted by surrounding basic residues of the N-terminal core domain. In its closed catalytically competent form, the C-terminal domain of LpxK undergoes a hinge motion to close around the nucleotide substrate upon binding (indicated with a curved arrow).

catalyst,^{15,16} presenting another mechanism by which base-mediated phosphate transfer may occur.

We present herein the kinetic characterization of purified LpxK and show that the enzyme catalyzes phosphate transfer through formation of a ternary complex at the membrane interface. Determination of steady-state kinetic parameters for a variety of active site point mutants and additional crystal structures of AMP-PCP-bound LpxK, ATP-bound LpxK in the open conformation (Scheme 1), and LpxK with an alternative P-loop conformation leads to the proposal of an overall catalytic mechanism. The detailed kinetic and structural characterization of LpxK reported here further elucidates the action of this unique P-loop kinase and provides additional groundwork for the continued development of LpxK into a viable antibiotic target.

■ EXPERIMENTAL PROCEDURES

Cloning and Expression of LpxK Constructs. All primers, plasmids, and strains referenced can be found in Tables S1 and S2 of the Supporting Information. Wild-type *A. aeolicus* LpxK was generated by growth of C41(DE3) cultures expressing construct pRPE7 and purified as previously described.^{9,17} Purified LpxK was stored in a buffer containing ~0.5% (w/v) dodecyl maltoside (DDM) (Anatrace, Maumee, OH), 750 mM NaCl, 20% (v/v) glycerol, and 50 mM HEPES (pH 8.0). QuikChange mutagenesis (Stratagene, La Jolla, CA) was employed to generate point mutants S49A, Y74A, D99A, D99N, D99E, E100A, E100Q, E100D, D138N, D139N, D260A, and H261A using the primer pairs listed in Table S1 of the Supporting Information and resulting in the plasmids listed in Table S2 of the Supporting Information. All constructs were validated by sequencing with primers prT7F and prT7R. Plasmids containing alanine point mutants for K51, T52, S53, D138, and D139 had been constructed in previous work.⁹ To generate partially purified LpxK point mutants, the plasmids were transformed into C41(DE3), expressed, and solubilized from membranes as previously described.^{9,18}

Assay and Kinetic Characterization of LpxK Activity. The lipid assay components ³²P-radiolabeled DSMP and nonradioactive DSMP were prepared as previously described.⁹

The standard assay conditions included 50 μM [³²P]DSMP (10000 cpm/nmol), 5 mM ATP, 5 mM MgCl₂, 50 mM Tris (pH 8.5), 0.5% (w/v) Triton X-100 (Thermo Scientific, Rockford, IL), 1 mg/mL BSA (Sigma-Aldrich, St. Louis, MO), 0.1 M NaCl, and *A. aeolicus* LpxK at 30 °C.⁹ Typically, LpxK was first diluted in 0.5% (w/v) Triton X-100, 0.5 M NaCl, and 50 mM Tris buffer before being diluted 5-fold (4 μL into 16 μL) into the assay to begin the reaction. Aliquots (4 μL) from the reaction mixtures were spotted onto 10 cm tall thin-layer chromatography (TLC) plates (EMD Chemicals, Gibbstown, NJ), developed in a chloroform/methanol/water/acetate [25:15:4:2 (v:v:v:v)] tank system, exposed to 35 cm × 43 cm Molecular Dynamics PhosphorImager screens, and scanned on a Storm 840 phosphorimager (GE Healthcare, Waukesha, WI).

To assess the pH dependence of the wild-type enzyme, the D99A point mutant, and the H261A point mutant, LpxK was assayed in the presence of a three-component buffer system consisting of 100 mM sodium acetate, 50 mM bis-Tris, and 50 mM Tris (pH 5–9.5) replacing the usual Tris buffer. The enzyme concentration in the assay was varied (between 0.3 and 3 nM for the wild-type enzyme) to keep conversion within the linear range. Enzyme, 100-fold concentrated with respect to the final assay condition, was first diluted 20-fold into 0.5% (w/v) Triton X-100, 0.5 M NaCl, and 50 mM pH buffer, and then 5-fold into the assay. The resulting curve was fit to eq 1 to assign pK_a and pK_b using Kaleideograph (Synergy Software, Reading, PA) as previously described.¹⁹

$$\nu = \frac{C}{1 + [\text{H}]/K_a + K_b/[\text{H}]} \quad (1)$$

where ν is the rate of the reaction, C is the pH-independent rate, $[\text{H}]$ is the hydrogen ion concentration, and K_a and K_b are the ionization constants of the acid and base species of LpxK, respectively.

To determine the detergent dependence of LpxK activity, the assay was conducted under the standard conditions with the Triton X-100 concentration varied from 0.05 to 62 mM. We were unable to assay LpxK at lower detergent concentrations because of the necessity of the detergent to solubilize the DSMP substrate in its stock solution. The enzyme concen-

Table 1. Data Collection and Refinement Statistics^a

	AMP-PCP–LpxK	ATP–LpxK	compact P-loop–LpxK
	Data Collection		
space group	<i>P</i> 2 ₁ 2 ₁ 2 ₁	<i>P</i> 2 ₁ 2 ₁ 2 ₁	<i>P</i> 2 ₁ 2 ₁ 2 ₁
unit cell [<i>a</i> , <i>b</i> , <i>c</i> (Å)]	66.1, 75.4, 104.6	62.7, 68.1, 105.9	62.1, 68.5, 107.6
wavelength (Å)	1.0	1.0	1.0
resolution (Å)	50.0–2.1 (2.14–2.10)	50.0–2.2 (2.24–2.20)	50.0–2.2 (2.24–2.20)
<i>R</i> _{merge}	0.059 (0.391)	0.073 (0.420)	0.046 (0.451)
<i>I</i> / <i>σ</i>	41.3 (2.8)	16.5 (2.3)	37.7 (2.6)
completeness (%)	92.3 (62.8)	97.1 (98.4)	97.4 (83.4)
redundancy	4.4 (3.1)	4.0 (3.6)	5.5 (4.2)
no. of reflections	129472	92699	128849
no. of unique reflections	29108	23000	23573
	Refinement		
<i>R</i> _{work} / <i>R</i> _{free} (%)	16.7/19.0	16.2/21.0	19.3/22.9
no. of atoms [average <i>B</i> factor (Å ²)]			
protein	2527 (50.4)	2585 (30.3)	2555 (71.7)
water	55 (41.7)	139 (28.6)	73 (53.6)
glycerol, MPD, HEPES	18 (89.4)	29 (44.3)	39 (96.3)
AMP-PCP	31 (32.1)	—	—
ATP	—	31 (20.6)	—
chloride	—	—	1 (60.5)
Ramachandran plot (%)			
favored	98.0	97.8	97.7
allowed	2.0	2.2	2.3
outlier	0.0	0.0	0.0
rmsd			
bond lengths (Å)	0.014	0.01	0.01
bond angles (deg)	1.48	1.16	1.15

^aValues in parentheses are those for the highest-resolution shell.

tration was varied between 0.5 and 10 nM to keep conversion within the linear range.

To assess which metal cations support LpxK activity, the enzyme concentrated at 270 nM was incubated in the standard enzyme dilution buffer plus 1 mM EDTA for 1 h at 4 °C. This solution was diluted 20-fold into dilution buffer containing 10 mM CaCl₂, CoCl₂, CuCl₂, FeCl₂, MgCl₂, MnCl₂, NiCl₂, or ZnCl₂ and incubated for 1 h at 4 °C. This enzyme solution was next diluted 5-fold into the standard assay without MgCl₂. Conversion of DSMP to lipid IV_A was assessed by TLC after 8 min. To determine whether excess Mg²⁺ inhibited LpxK activity, the enzyme was assayed between 0.3 and 8 nM under the standard assay condition with 5 mM ATP and increasing amounts of MgCl₂ ranging from 0.015 to 128 mM.

To examine whether excess salt inhibited LpxK activity, we performed the standard assay in the presence of 0–800 mM NaCl or KBr. The enzyme first diluted to 5 nM in 0.5% (w/v) Triton X-100 and 50 mM Tris buffer (pH 8.5) was immediately diluted 5-fold into the assay and specific activity assessed.

Determination of Apparent Steady-State Kinetic Parameters. The apparent kinetic parameters for the ATP/Mg²⁺ complex were determined by performing the standard assay in triplicate at a fixed DSMP concentration of 50 μM while varying the concentrations of ATP and MgCl₂ from 0.3 to 10 mM. The LpxK concentration in these assays varied between 0.3 and 2 nM. Conversely, to determine the apparent kinetic parameters for DSMP, the ATP/MgCl₂ concentration was fixed at 5 mM while the lipid concentration varied from 1.56 to 100 μM. Both curves were fit to the Michaelis–Menten equation using KadeidaGraph (Synergy Software, Reading, PA) to determine the apparent *K*_M and *k*_{cat} with respect to each

substrate. For the determination of apparent kinetic parameters of the solubilized point mutants, the ATP/MgCl₂ concentration was varied from 0.3 to 15 mM at a fixed DSMP concentration of 50 μM and again fit to the Michaelis–Menten equation. The enzyme concentration was varied to capture the linear range of activity for each mutant.

To analyze LpxK activity through bisubstrate kinetics, the enzyme was assayed with the ATP/MgCl₂ concentration varied from 0.3 to 10 mM at four fixed DSMP concentrations (2.5, 5, 15, and 50 μM). The data were fit to equations describing either a ping-pong mechanism (eq 2) or a sequential mechanism (eq 3) as has been described previously, using PRISM (GraphPad Software, La Jolla, CA).²⁰

$$v = \frac{V_m AB}{K_{Ma} B + K_{Mb} A + AB} \quad (2)$$

$$v = \frac{V_m AB}{K_{Ma} B + K_{Mb} A + K_{ia} K_{Mb} + AB} \quad (3)$$

where *A* and *B* represent the concentrations of the two substrates, *K*_{Ma} is the *K*_M for substrate A, *K*_{Mb} is the *K*_M for substrate B, *K*_{ia} is the dissociation constant for substrate A, *v* is the reaction velocity, and *V*_m is the maximal velocity.

Crystallization and Structure Determination of LpxK in Complex with AMP-PCP, ATP, and an Alternate P-Loop Conformation. Crystals were grown in 24-well trays (Hampton Research, Aliso Viejo, CA) using the sitting drop vapor diffusion method. All conditions included 2-methyl-2,4-pentanediol (MPD) and HEPES (Qiagen, Valencia, CA), with a well volume of 700 μL and a drop volume of 10 μL incubated at 20 °C. All crystals were harvested after growing for 1 month

and were immediately flash-frozen in liquid nitrogen after being looped. Following collection, all data were reduced and scaled using HKL-2000,²¹ and the structure was determined by molecular replacement using PHASER within the PHENIX software suite.²² The model was manually rebuilt in COOT²³ between rounds of iterative maximum-likelihood refinement in PHENIX, which included TLS options. Using an electron density acceptance criterion of $d \geq 3\sigma(d)$ in the $F_o - F_c$ difference electron density map, ligands (AMP-PCP, ATP, chloride, HEPES, MPD, or glycerol) were added to the respective models. The overall structures were validated using MOLPROBITY²⁴ and imaged in PyMOL.²⁵ Data collection and refinement statistics are listed in Table 1.

Rod-shaped crystals ($0.2 \text{ mm} \times 0.05 \text{ mm} \times 0.05 \text{ mm}$) resulted when LpxK was incubated with AMP-PCP (Sigma-Aldrich). The drop contained four parts of a reservoir solution consisting of 50% (v/v) MPD and 0.1 M HEPES (pH 7.5) and one part of a protein solution containing 13 mg/mL LpxK, 4.3 mM AMP-PCP, 1 mM EDTA, 0.5% (w/v) DDM, 540 mM NaCl, 14% (v/v) glycerol, and 35 mM HEPES (pH 8.0). Similar crystals resulted after a round of microseeding in which 1 μL of a seed stock (one crystal dissolved in 0.5 mL of reservoir solution) was added to the drop. The harvested crystal diffracted to 2.1 \AA and belonged to the $P2_12_12_1$ space group ($a = 66.1 \text{ \AA}$, $b = 75.4 \text{ \AA}$, and $c = 104.6 \text{ \AA}$). Data were collected at a single wavelength (1.0 \AA) at the Southeast Regional Collaborative Access Team (SERCAT) 22-ID beamline at the Advanced Photon Source (APS, Argonne National Laboratory, Argonne, IL). The structure was determined by molecular replacement using the previously reported ADP/Mg²⁺-LpxK structure (PDB entry 4EHY) as the search model with all ligands removed, and AMP-PCP was subsequently added to the model.

Rod-shaped crystals ($0.25 \text{ mm} \times 0.05 \text{ mm} \times 0.05 \text{ mm}$) resulted when LpxK was incubated with ATP. The drop contained 17 parts of a reservoir solution consisting of 60% (v/v) MPD and 0.1 M HEPES (pH 7.5) and three parts of a protein solution containing 7.4 mg/mL LpxK, 10 mM ATP, 1 mM EDTA, 0.35% (w/v) DDM, 700 mM NaCl, 18.5% (v/v) glycerol, and 45 mM HEPES (pH 8.0). A harvested crystal diffracted to 2.2 \AA , and data were collected at a single wavelength (1.0 \AA) at the SERCAT beamline in the $P2_12_12_1$ space group ($a = 62.7 \text{ \AA}$, $b = 68.1 \text{ \AA}$, and $c = 105.9 \text{ \AA}$). The structure was determined using the previously reported apo LpxK structure (PDB entry 4EHX) as the molecular replacement search model, and ATP was subsequently added to the structure.

Boxy rod-shaped crystals ($0.15 \text{ mm} \times 0.1 \text{ mm} \times 0.1 \text{ mm}$) resulted from a drop that contained three parts of a reservoir solution consisting of 40% (v/v) MPD and 0.1 M HEPES (pH 7.5) and one part of a protein solution containing 8.3 mg/mL LpxK, 4 mM methyl 2-acetamido-2-deoxy- β -D-glucopyranoside,²⁶ 0.35% (w/v) DDM, 625 mM NaCl, 17% (v/v) glycerol, and 45 mM HEPES (pH 8.0). A harvested crystal diffracted to 2.2 \AA , and data were collected at a single wavelength (1.0 \AA) at the SERCAT beamline in the $P2_12_12_1$ space group ($a = 62.1 \text{ \AA}$, $b = 68.5 \text{ \AA}$, and $c = 107.6 \text{ \AA}$). The structure was determined using the apo LpxK structure (PDB entry 4EHX) as the molecular replacement search model, and spherical active site density refined well as a chloride ion.

RESULTS

pH, Detergent, and Metal Dependence of LpxK Activity

Activity. The *A. aeolicus* LpxK assay was performed in triplicate in the presence of a triple-buffer system at various pH values to determine the effect of pH on overall activity. LpxK was found to tolerate a broad pH optimum with a pK_a of 6.6 ± 0.1 and a pK_b of 9.7 ± 0.1 (Figure 1A). Inactivation of

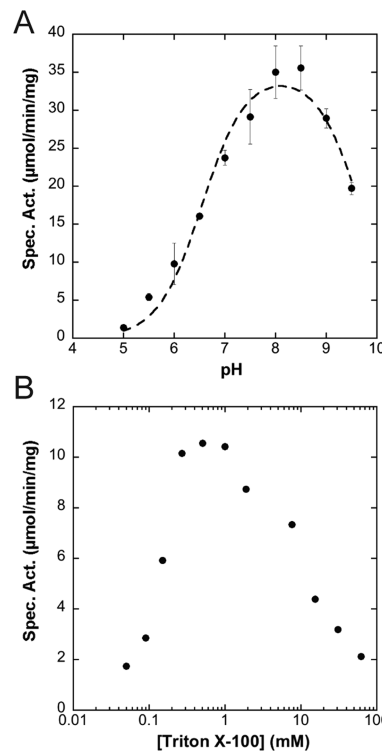


Figure 1. pH and detergent dependence of LpxK activity. (A) *A. aeolicus* LpxK was assayed in triplicate in a triple-buffer system (100 mM sodium acetate, 50 mM Tris, and 50 mM bis-Tris) at the indicated pH values and specific activity assessed. A pK_a of 6.6 ± 0.1 and a pK_b of 9.7 ± 0.1 were calculated. (B) The enzyme was also assayed under the standard assay conditions in the presence of 0.05–62 mM Triton X-100 and activity assessed. Both the detergent requirement and the reduced activity with increased micellar surface area indicate that LpxK-catalyzed phosphorylation of DSMP occurs at the micelle surface.

the enzyme at low pH was reversible as this enzyme could be rediluted into a buffer with a pH of 8 to restore full activity (data not shown). LpxK was also assayed in the presence of increasing amounts of detergent (0.05–62 mM) while the DSMP concentration was kept fixed at 50 μM to determine the effects of increasing micelle surface area on activity.²⁷ LpxK achieved maximal activity as the amount of Triton X-100 in the assay overcame the critical micelle concentration ($\sim 0.2 \text{ mM}$), followed by a decay in activity as the micelle surface area increased with the amount of detergent (Figure 1B). To assess the metal dependence of kinase activity, LpxK was incubated with EDTA, diluted into buffer containing select cations, and further diluted into buffer containing the rest of the reaction components. Activity was stimulated by the presence of Mg²⁺, Co²⁺, and Mn²⁺, while significantly less phosphoryl transfer was observed when LpxK was incubated with Ca²⁺, Ni²⁺, Cu²⁺, Zn²⁺, or Fe³⁺ (Figure 2A). Almost no activity was observed for the enzyme as purified without the addition of any metals. To

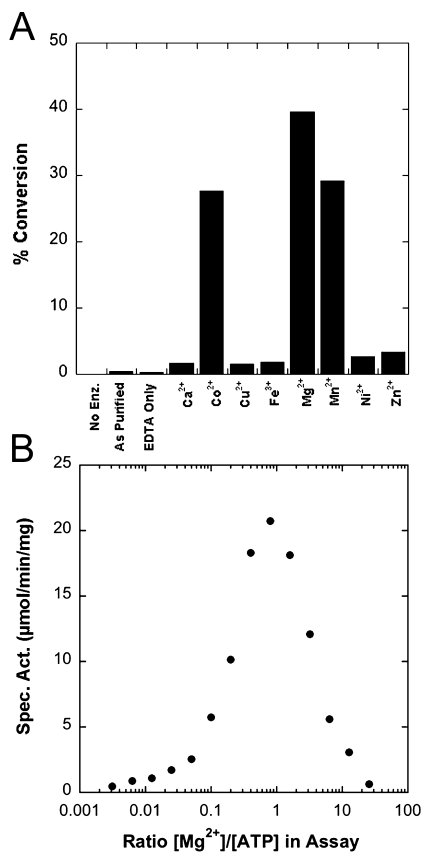


Figure 2. Metal dependence of LpxK activity. (A) Purified LpxK, which was first incubated with EDTA, was then diluted into assay buffer containing 2 mM ATP and the indicated cation, and the reaction was quenched by spotting the mixture on a TLC plate after 8 min. (B) The standard assay was performed in the presence of 5 mM ATP and 0.015–128 mM Mg²⁺. The cation is necessary for activity but becomes inhibitory at high concentrations with respect to ATP.

determine whether excess Mg²⁺ in the assay was inhibitory with respect to activity, LpxK was assayed under the standard assay condition in the presence of 0.015–128 mM cation. Optimal activity was observed at an equimolar ratio of ATP to Mg²⁺, with a decrease in activity with larger amounts of the divalent cation (Figure 2B).

Apparent Steady-State Kinetic Parameters for LpxK Activity Support the Formation of a Ternary LpxK–ATP/Mg²⁺–DSMP Complex. Because of the surface dilution effects of the mixed micelle assay, all kinetic parameters are deemed “apparent” (Figure 1B).²⁷ The velocity of the *A. aeolicus* LpxK phosphoryl transfer reaction was assessed for various concentrations of ATP and Mg²⁺ held in a 1:1 ratio, at a fixed concentration of DSMP. The K_M for the nucleotide/cation complex was determined to be 1.6 ± 0.2 mM with a k_{cat} of 12.3 ± 0.4 s⁻¹ (Figure 3A). The kinetic parameters for the lipid substrate DSMP were also determined by varying the lipid concentration in the assay at saturating amounts of ATP/Mg²⁺, yielding a K_M of 7.0 ± 0.3 μM and a k_{cat} of 9.2 ± 0.1 s⁻¹ (Figure 3B).

The LpxK reaction was further analyzed via bisubstrate kinetics to determine whether the reaction proceeds through a ping-pong-type mechanism (transient existence of a phosphoenzyme intermediate) or a sequential mechanism (formation of a ternary complex).²⁰ Lineweaver–Burk plots constructed for varied ATP/MgCl₂ concentrations (held at a 1:1 ratio) at four

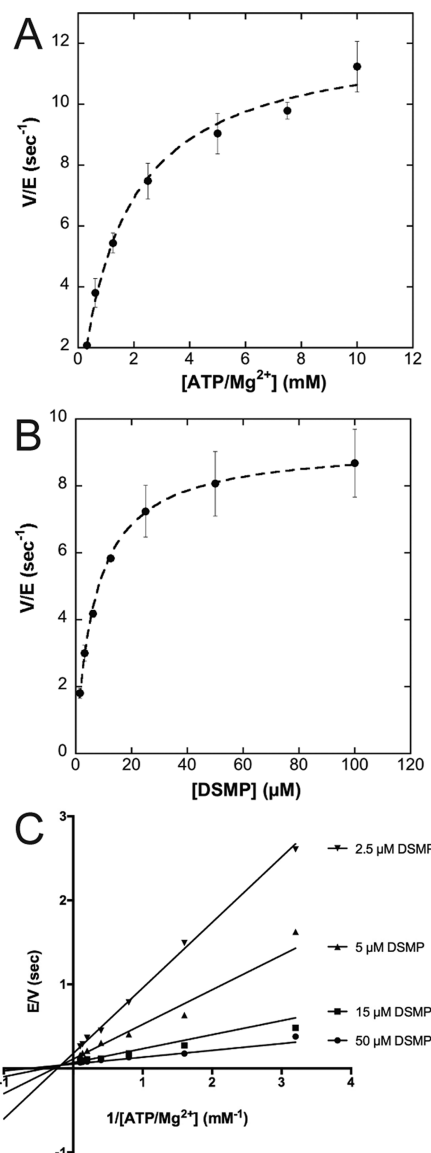


Figure 3. Apparent kinetic parameters and bisubstrate kinetic analysis of LpxK. (A) *A. aeolicus* LpxK was assayed at a fixed DSMP concentration of 50 μM and varied amounts of ATP/Mg²⁺ ranging from 0.3 to 10 mM. The apparent K_M for ATP/Mg²⁺ was determined to be 1.6 ± 0.2 mM with a k_{cat} of 12.3 ± 0.4 s⁻¹. (B) The concentration of ATP/Mg²⁺ in the assay was fixed at 5 mM, while the concentration of DSMP was varied between 1.56 and 100 μM. The apparent K_M for DSMP was determined to be 7.0 ± 0.3 μM with a k_{cat} of 9.2 ± 0.1 s⁻¹. (C) In this series of assays, the concentration of ATP/Mg²⁺ was varied between 0.3 and 10 mM for four fixed concentrations of the DSMP substrate (2.5, 5, 15, and 50 μM). The data were fit by a nonlinear least-squares method to a sequential mechanism.

fixed concentrations of the lipid substrate were overlaid to reveal intersecting lines, indicating the necessity of the formation of a ternary complex for catalysis (Figure 3C). The global fit of the data for a sequential mechanism was favored over a ping-pong-type mechanism with a V_m of 18.0 ± 0.7 s⁻¹, a K_{Ma} of 1.0 ± 0.2 mM, a K_{Mb} of 7 ± 1 μM, and a K_{ia} of 3.1 ± 0.8 mM, where substrate A is ATP/Mg²⁺ and substrate B is DSMP.

Crystal Structure of AMP-PCP-Bound LpxK. To identify the precatalytic position of the ATP γ-phosphate in LpxK, cocrystals in complex with the nonhydrolyzable analogue AMP-PCP were generated, and the structure was determined via

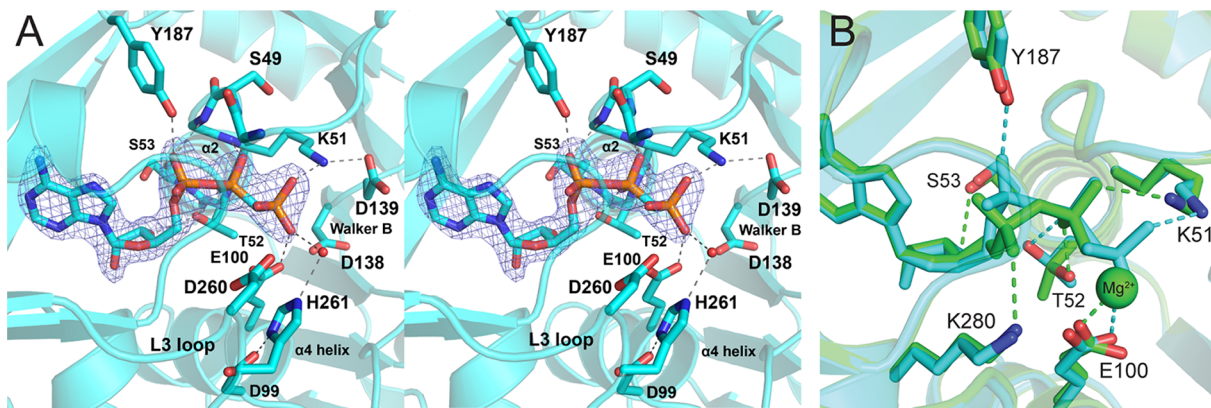


Figure 4. Active site of LpxK bound to AMP-PCP. (A) Active site stereoview revealing AMP-PCP bound in the closed enzyme conformation between the C-terminal domain and β -linker. Water (red sphere) and putative hydrogen bonds (dashed lines) are shown. Simulated annealing omit electron density for AMP-PCP (mesh) was calculated with $F_o - F_c$ coefficients, contoured at 4σ . (B) Overlay of AMP-PCP-bound (cyan) and ADP/ Mg^{2+} -bound (PDB entry 4EHY) (green) LpxK structures. Side chains and hydrogen bonds (dashed lines) are colored accordingly. The Mg^{2+} ion of the ADP/ Mg^{2+} structure is bound at the same site as the γ -phosphate of AMP-PCP.

molecular replacement (Table 1). The AMP-PCP-containing structure shows the analogue bound to the enzyme in the closed form (Scheme 1), with the β -phosphate sitting at the base of helix $\alpha 2$ (Figure 4A). The AMP-PCP structure overlays well with the structure previously determined for the postcatalytic ADP/ Mg^{2+} -bound LpxK structure with three differences⁹ (Figure 4B). First, the position of the α -phosphate is shifted slightly between the two structures, the ADP/ Mg^{2+} α -phosphate favoring an interaction with the side chain of K280 and AMP-PCP favoring hydrogen bonding to Y187. Second, the γ -phosphate of AMP-PCP resides in a position occupied by the cation in the ADP/ Mg^{2+} structure, participating in hydrogen bonding interactions with E100 of helix $\alpha 4$ and K51 of the P-loop motif. Third, T52 forms a hydrogen bond with a ribose hydroxyl, which is bound to S53 in the ADP/ Mg^{2+} structure. In both the ADP/ Mg^{2+} and AMP-PCP crystal structures, the side chain of D99 is bonded to H261 of the L3 loop, which is reminiscent of the charge relay system of serine proteases²⁸ (Figure 4A). The γ -phosphate of AMP-PCP is well-positioned for transfer as it is directly adjacent to the putative DSMP-binding pocket on the underside of the N-terminal domain.

Kinetic Parameter Perturbations of LpxK Active Site Point Mutants. To gain insight into the LpxK catalytic mechanism, point mutants of various conserved active site residues informed by LpxK structures with bound nucleotide were generated and partially purified through solubilization from membranes of the expression strain. All point mutants were expressed at similar levels and behaved like wild type throughout the partial purification as judged by SDS-PAGE (data not shown). Apparent kinetic parameters for ATP/ Mg^{2+} were determined for the wild-type enzyme along with each point mutant to assess whether these residues have a catalytic role and/or assist in binding the nucleotide or cation substrate. The results are listed in Table 2.

Alanine mutants of Walker A motif residues S49 and S53, implicated in ATP binding through interaction with the β -phosphate and a ribose hydroxyl (Figure 4), had little relative effect on k_{cat} while showing increased K_M values for the nucleotide/cation complex 2.3- and 5-fold above that of the wild type, respectively. The K51A mutant had a much more significant effect on k_{cat} (3000-fold), while displaying an only slight ATP/ Mg^{2+} K_M increase. The T52A mutant also led to a

Table 2. Kinetic Parameters of LpxK Point Mutants with Respect to ATP/ Mg^{2+}

	apparent K_M (mM)	x-fold increase in K_M	apparent k_{cat} (s ⁻¹)	x-fold decrease in k_{cat}
WT	1.2 ± 0.2	1.0	3.9 ± 0.2	1.0
S49A	2.7 ± 0.3	2.3	3.9 ± 0.1	1.0
K51A	1.5 ± 0.4	1.3	$(1.3 \pm 0.1) \times 10^{-3}$	3000
T52A	2.2 ± 0.3	1.8	$(1.3 \pm 0.1) \times 10^{-3}$	3000
S53A	6 ± 1	5	$(4.7 \pm 0.6) \times 10^{-1}$	8.3
Y74A	1.7 ± 0.3	1.4	$(2.2 \pm 0.1) \times 10^{-2}$	180
D99A	2.8 ± 0.5	2.3	$(1.5 \pm 0.1) \times 10^{-3}$	2600
D99N	1.1 ± 0.2	1.0	$(3.5 \pm 0.2) \times 10^{-4}$	11000
D99E	2.3 ± 0.2	1.9	$(5.0 \pm 0.2) \times 10^{-2}$	78
E100A	1.9 ± 0.5	1.6	$(2.9 \pm 0.2) \times 10^{-3}$	1300
E100Q	2.9 ± 0.4	2.4	$(4.8 \pm 0.2) \times 10^{-4}$	8100
E100D	2.0 ± 0.3	1.7	$(2.7 \pm 0.1) \times 10^{-3}$	1400
D138A	4.0 ± 0.6	3.3	$(8.3 \pm 0.4) \times 10^{-4}$	4700
D138N	3.2 ± 0.7	2.7	$(5.7 \pm 0.5) \times 10^{-2}$	68
D139A	5 ± 1	4	$(4.8 \pm 0.5) \times 10^{-4}$	8100
D139N	1.4 ± 0.3	1.2	$(7.6 \pm 0.5) \times 10^{-3}$	510
D260A	1.6 ± 0.3	1.3	$(7.3 \pm 0.4) \times 10^{-2}$	53
H261A	1.3 ± 0.2	1.1	$(4.6 \pm 0.2) \times 10^{-3}$	850

large decrease in the rate of turnover (3000-fold) and a modest ATP/ Mg^{2+} K_M increase (1.8-fold).

Both alanine and asparagine mutants of Walker B carboxylate-containing residues D138 and D139 were generated. The alanine mutants of both residues had significantly decreased k_{cat} values (4700- and 8100-fold compared to that of the wild type, respectively) along with increases in ATP/ Mg^{2+} K_M (3.3- and 4-fold, respectively). The asparagine mutants of these residues showed some restoration of activity when compared to the alanine mutants (only 68- and 510-fold losses of activity for D138N and D139N, respectively, compared to that of the wild type). The K_M for the nucleotide/cation complex is recovered as well, to a value 2.7-fold higher than that of WT for the D138N mutant and near WT levels for D139N.

Conserved carboxylate-containing residues of helix $\alpha 4$ were also deemed to be critical for activity. D99, whose side chain is bonded to H261 of the L3 loop in the closed conformation of LpxK (Figure 4A), was mutated to alanine, asparagine, and glutamate. The alanine mutant of this residue resulted in a

2600-fold decrease in k_{cat} and a 2.3-fold increase in ATP/Mg²⁺ K_M . Interestingly, the asparagine mutant of this same residue displayed a further decreased k_{cat} (11000-fold) with a full restoration of K_M for the nucleotide/cation complex. The glutamate mutant of D99 results in an only 78-fold decrease in velocity with a 1.9-fold increase in K_M . Because the proper ionization state of this residue seems to be crucial to efficient turnover, the pH dependence of the D99A point mutant was assessed, revealing a shift in pK_a from 6.6 ± 0.1 to 5.8 ± 0.1 with respect to the wild-type enzyme while leaving the pK_b undisturbed at 9.6 ± 0.1 (Figure 5A). It is important to note

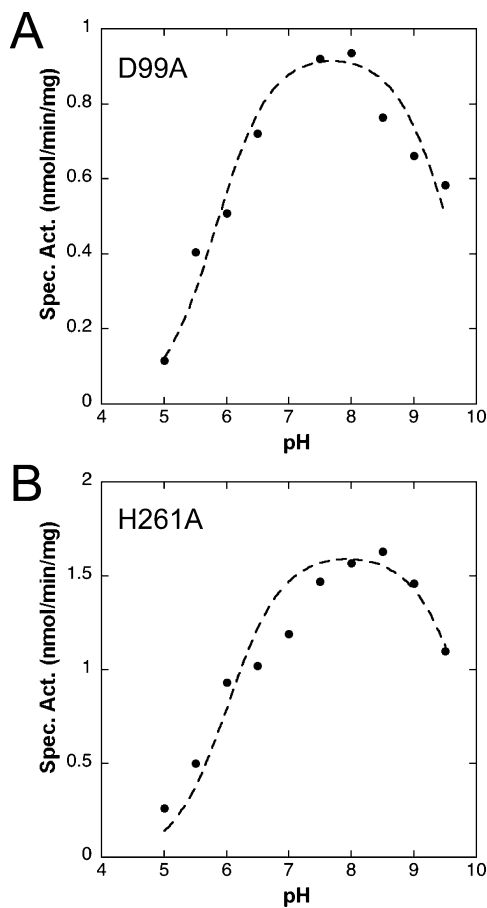


Figure 5. pH dependence of active site point mutants. (A) The D99A LpxK mutant was assayed in a triple-buffer system (100 mM sodium acetate, 50 mM Tris, and 50 mM bis-Tris) at the indicated pH values and specific activity assessed. A pK_a of 5.8 ± 0.1 and a pK_b of 9.6 ± 0.1 were calculated. (B) In the same manner, the pH dependence of the H261A mutant was analyzed, resulting in pK_a and pK_b values of 6.0 ± 0.1 and 9.9 ± 0.2 , respectively.

that because of potential chemical rescue with acetate found in the pH buffer, the apparent pK_a and pK_b for this mutant may be slightly altered from the true values. The E100 residue was mutated to alanine, glutamine, and aspartate, which resulted in 1300-, 8100-, and 1400-fold decreases in k_{cat} , respectively. The ATP/Mg²⁺ K_M values for the E100 mutants are increased 1.6-, 2.4-, and 1.7-fold for the alanine, glutamine, and asparate mutants, respectively. The pattern from the D99 mutants was preserved, where the carboxamide mutant showed a more significantly decreased k_{cat} when compared to that of the alanine mutant, but is partially recovered with the restoration of the carboxylate functional group with E100D.

Further alanine point mutants were generated for other residues that occupy the active site. Y74 lines the putative DSMP-binding pocket but is close enough to the active site to participate in catalysis. The alanine point mutant of Y74 resulted in a 1.4-fold increase in ATP/Mg²⁺ K_M and a 180-fold decrease in k_{cat} . An alanine mutant of D260 of loop L3 (Figure 4A) displays a slightly increased nucleotide/cation K_M (1.3-fold) and a 53-fold decreased k_{cat} . The alanine mutant of H261, a residue of loop L3 that is hydrogen bonded to D99 of helix $\alpha 4$, shows little effect on the nucleotide/cation K_M , but k_{cat} is decreased 850-fold, indicating the imidazole moiety's importance for kinase activity. The pH dependence the H261A mutant was also assessed because of its contact with the critical D99 residue. pK_a and pK_b were calculated to be 6.0 ± 0.1 and 9.9 ± 0.2 , respectively, revealing a pattern similar to that of the D99A mutant where the pK_a is downshifted with respect to that of the wild type (Figure 5B).

Crystal Structure of ATP Bound to "Open" Form LpxK.

In an attempt to obtain an ATP-bound structure, LpxK was incubated with EDTA and ATP under the MPD condition. Rod-shaped crystals were obtained, which surprisingly showed ATP bound in the open form of the enzyme (Scheme 1 and Figure 6A). This ATP does not occupy the same binding site as AMP-PCP, likely because in the open form, the C-terminal domain is not closed around the nucleotide. Instead, ATP is found in a "bent" conformation, which may represent the binding state of the nucleotide before closure of the C-terminal domain. A well-ordered MPD molecule is also found bound in this pocket. The conformation of ATP consists of the α -phosphate positioned at the base of helix $\alpha 2$, the site normally occupied by the β -phosphate in both the ATP/Mg²⁺-bound⁹ and AMP-PCP-bound structures.

Comparisons of the AMP-PCP- and ATP-bound LpxK structures reveal that besides the large difference in the position of the C-terminal domain (Scheme 1), specific residues show significant shifts (Figure 6B). Q240 trades a hydrogen bond with the α -phosphate of ATP for the adenine ring of AMP-PCP. The F296 side chain is rotated 180° to mediate a π -stacking interaction with this same adenine. Other side chains (Y187, S53, R206, and T52) retain the same relative positioning but trade binding partners between the two structures. Y187 participates in a hydrogen bond with the β -phosphate in the ATP structure but switches to the α -phosphate of AMP-PCP. S53 is bound to an adenine nitrogen atom of ATP but contacts a ribose hydroxyl in the AMP-PCP structure. R206 trades a bond with the α -phosphate of ADP for the adenine ring, and T52 binds the γ -phosphate of ATP only to switch to the β -phosphate and a ribose hydroxyl in the AMP-PCP structure.

Crystal Structure of a "Compact" P-Loop Conformation.

Under the same drop condition that had produced apo LpxK crystals⁹ except for a slightly higher salt concentration, boxy rod-shaped crystals of the same space group and unit cell dimensions appeared, which when the structure was determined were observed to have an unaltered overall appearance except for the position of the P-loop (Figure 7A). In these crystals, the P-loop is compact, with residues G48, S49, and G50 of the P-loop shifted to complete another turn of the $\alpha 2$ helix. Pinning down these residues at the base of the helix is spherical density that, given the high chloride concentration in the drop (~160 mM) and the dipole properties of helices, was assigned as a chloride ion. This structure may explain weak positive difference density seen in the apo LpxK structure (PDB

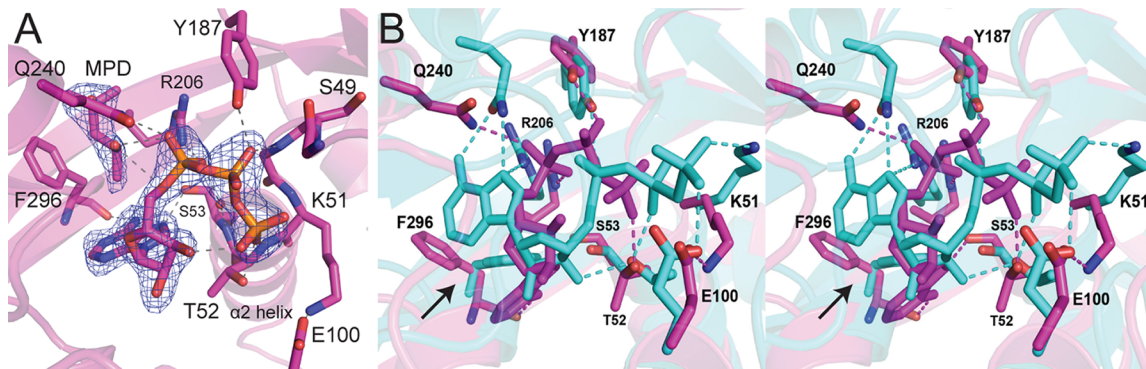


Figure 6. Active site of ATP-bound *A. aeolicus* LpxK in the open form. (A) Simulated annealing omit electron density for ATP and MPD (mesh) in the ATP-bound structure was calculated using $F_o - F_c$ coefficients, contoured at 4σ . The bent ATP molecule is bound to the open, normally apo conformation of the enzyme. Dashed lines indicate hydrogen bonds. (B) A stereoview of the overlay of AMP-PCP-bound (cyan) and ATP-bound (magenta) LpxK structures reveals a shift in nucleotide binding upon domain closure. Side chains and hydrogen bonds are colored accordingly. Side chain rotation of F296 between the two structures is indicated with an arrow.

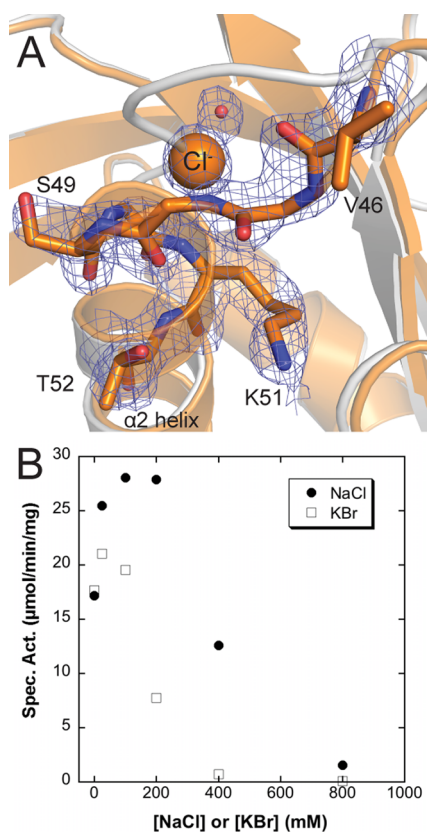


Figure 7. Structural basis for anion inhibition of LpxK. (A) The compact P-loop conformation along with a chloride ion (orange sphere) and a water molecule (red sphere) likely displays an inactive P-loop conformer. Electron density calculated using $2F_o - F_c$ coefficients contoured at 2σ is shown (mesh). To note the P-loop shift, the apo LpxK cartoon is overlaid (gray) (PDB entry 4EHX). (B) Salt dependence of LpxK activity. The standard assay was performed in the presence of 0–0.8 M NaCl or KBr. Though having some salt (either NaCl or KBr) in the assay condition is stimulatory, excess salt becomes inhibitory. This result may represent the biochemical consequence of the compact P-loop conformation observed with a chloride ion obstructing the active site.

entry 4EHX), as the P-loop may exist in a semidynamic state alternating between these two conformations.⁹ To determine the effect of salt on activity, the assay was performed in the

presence of increasing NaCl and KBr concentrations (Figure 7B). Though both salts initially stimulated activity up to concentrations of 50–100 mM, excess salt was found to become inhibitory.

DISCUSSION

LpxK catalyzes the sixth step in the lipid A biosynthetic pathway, and its activity is essential to bacterial viability.²⁹ The crystal structures of *A. aeolicus* LpxK in both apo and ADP/Mg²⁺-bound forms have been previously reported, revealing a significant domain rearrangement upon nucleotide binding (Scheme 1).⁹ To improve our understanding of the catalytic mechanism of LpxK and the molecular basis for phosphoryl transfer, we have performed detailed kinetic characterization of the kinase from *A. aeolicus* and determined additional crystal structures of LpxK bound to AMP-PCP and ATP, as well as an open form of LpxK with an unusual compact P-loop conformation.

Biochemical Characteristics of LpxK Differentiate This Membrane-Bound Kinase from Its Cytosolic Relatives. We kinetically characterized LpxK to understand how membrane-associated kinases function at the lipid interface. LpxK's lipid kinase activity requires the presence of detergents at concentrations above the CMC and is susceptible to surface dilution (Figure 1B). The observed surface dilution effect supports the notion that catalysis is occurring at the membrane interface.²⁷ This notion correlates with previously published crystal structures of LpxK that revealed the presence of an extended, hydrophobic N-terminal helix, which we proposed functions to associate LpxK with the membrane.

Apart from the requirement of detergent, LpxK displays a bell-shaped, pH-rate profile that maximizes at slightly basic pH (Figure 1A), distinguishing it from other P-loop kinases that function best in an acidic environment.³⁰ Because of the limitations of pH versus activity assays, we have been cautious not to overinterpret the pK_a and pK_b values obtained as they may not represent a single ionizable group or take into account the pH dependence of the substrate K_M values.³¹ However, the restoration of activity upon return to neutral pH after incubation and low pH suggests that protonation of necessary active site residues for substrate binding and/or catalysis may reversibly inactivate the enzyme. LpxK can utilize magnesium, cobalt, or manganese as metal cofactors, albeit Mg²⁺ is likely the preferred divalent cation (Figure 2A). Excess magnesium is

inhibitory, as has been described for other kinases, perhaps because of the existence of a second inhibitory cation binding site as has been described for many protein kinases (Figure 2B).³² For LpxK, the previously observed putative “postcatalytic” binding site of Mg²⁺ may be inhibitory, effectively trapping the ADP product in the active site (Figure 4B).⁹

Apparent kinetic parameters for both substrates were determined for *A. aeolicus* LpxK (Figure 3). The K_M for ATP/Mg²⁺ was on the same order of magnitude compared with those of other membrane-bound lipid kinases.³³ The K_M for DSMP was slightly lower than the reported K_M values for KdtA and LpxL, which also utilize tetraacylated lipid substrates in the lipid A biosynthetic pathway.^{34,35} It is generally accepted that P-loop kinases catalyze direct transfer of the phosphate of ATP,^{4,12,13} a property of LpxK that we investigated using steady-state kinetics. Despite the low degree of homology of LpxK to other P-loop kinase family members in both sequence (outside the Walker motifs) and structure, these enzymes do share the necessity of forming a ternary complex (Figure 3C).

Structural Insights into Nucleotide Binding and Inhibitory Conformations of the LpxK P-Loop. The AMP-PCP–LpxK structure is consistent with the previous proposal that the precatalytic position of the γ -phosphate is bound to E100 of helix α 4, and that the likely catalytic coordination of the Mg²⁺ ion involves T52, E100, and D138 along with the two terminal phosphates of ATP (Figure 4A and Scheme 2).⁹ Though this structure is informative, the binding of the Mg²⁺ ion may further alter the geometry of the nucleotide, as made evident by comparison with the ADP/Mg²⁺ structure (Figure 4B). The structure of LpxK with ATP bound in the open apo enzyme conformation (Scheme 1) reveals a

potential precatalytic binding site of the nucleotide prior to formation of the catalytically competent closed form (Figure 6). Because there was EDTA included in the drop to prevent hydrolysis of ATP, it stands to reason that an unoccupied Mg²⁺ binding site could be associated with this particular conformation of the nucleotide, altering its overall geometry when the cation is present. Nevertheless, the ATP-bound, AMP-PCP-bound, and previously reported ADP/Mg²⁺-bound⁹ structures may provide a glimpse of nucleotide–enzyme interactions before, during, and after catalysis has occurred.

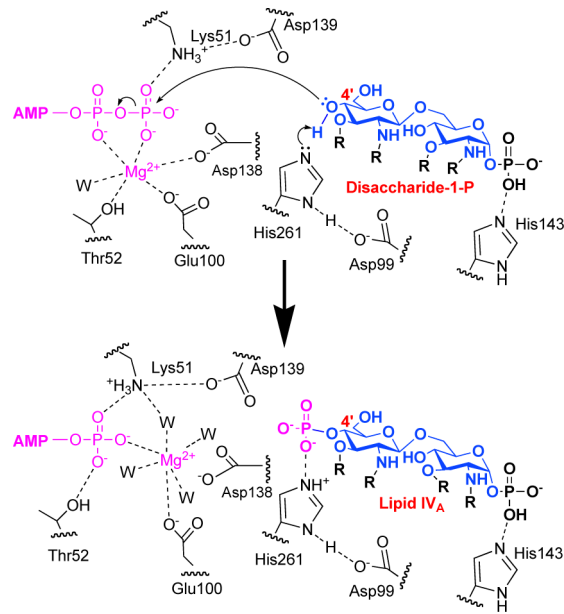
The third structure reported in this work shows a chloride ion pinning the P-loop onto helix α 2, causing LpxK to adopt a seemingly inactive conformation and potentially demonstrating how excess salt in the assay is inhibitory (Figure 7). Because the detergent in the assay system (Triton X-100) has a neutral headgroup, inhibition at high salt concentrations is likely a direct effect of the ions interacting with the protein itself and not a result of separation of LpxK from the micelle surface, which under the assay condition may be relying solely on the hydrophobic N-terminal helix for micelle attachment. Thus, this compact P-loop structure reveals an intriguing mode of allosteric regulation of LpxK activity and may provide important insights into the development of allosteric LpxK inhibitors.

Roles of Active Site Residues in LpxK Catalysis.

Extensive point mutagenesis was performed on active site residues to gain insight into their roles in kinase activity (Table 2). Overall, most of the point mutants resulted in significant effects on the apparent k_{cat} , likely because even small perturbations in the proper alignment of the substrates can significantly affect catalytic efficiency. Residues S49 and S53, based on the kinetic data, appear to be primarily involved in ATP binding because alanine mutants of these residues showed significantly affected K_M values for the nucleotide/cation with a modest decrease in the relative k_{cat} . All of the residues that are implicated in holding Mg²⁺ in its catalytically competent conformation (T52, E100, and D138) have elevated ATP/Mg²⁺ K_M values when they are mutated to alanine, though the largest increase for this parameter is seen for the D138A mutant. The Y74A mutant had a relatively modest effect on k_{cat} with only slight shifts in K_M for nucleotide. Y74 lines the putative DSMP binding pocket and may play a greater role in lipid binding. The alanine mutant of K51, one of the most highly conserved residues of the P-loop kinase superfamily, showed little effect on the nucleotide/cation apparent K_M and a large decrease in k_{cat} , highlighting its primarily catalytic role.¹²

In some P-loop kinases related to LpxK, the existence of a catalytic base has been postulated to assist in phosphoryl transfer.¹⁴ The crystal structure of LpxK with bound AMP-PCP reveals several possibilities for a putative catalytic base that is responsible for the activation of the 4'-hydroxyl group of DSMP. E100 of helix α 4, D139 of the Walker B motif, D260 of the L3 loop, and H261 of this same loop are all well-positioned within the active site near the γ -phosphate of ATP and the putative binding locale of the 4'-hydroxyl of DSMP (Figure 4A). Of the two residues in the L3 loop, H261 appears to be more catalytically relevant than D260 because when the alanine mutants of these residues are compared, a loss of the imidazole ring affects catalysis much more dramatically (Table 2). Perhaps the most intriguing possibility, given the observed interaction between the carboxylate group of D99 and the imidazole ring of H261 (Figure 4A), is the formation of an aspartate-histidine dyad, which is commonly seen in the charge

Scheme 2. Proposed Catalytic Mechanism of LpxK^a



^aH261 acts as the catalytic base that is activated by an interaction with D99, providing a proton sink. H261 abstracts a proton from the 4'-hydroxyl of DSMP, which undergoes nucleophilic attack of the γ -phosphate of ATP (pink). The Mg²⁺ ion (pink) shifts to its postcatalysis position between E100 and the β -phosphate of ADP and becomes solvated by additional water molecules. The acyl chains (R) on the glucosamine backbone (blue) represent (R)-3-hydroxymyristic acid.

relay systems found in serine proteases.²⁸ The use of a histidine as a general base has not been previously reported for any characterized P-loop kinase family member, though a few unrelated kinases and sulfotransferases are thought to use this amino acid as a base catalyst.^{15,16} In this scenario, D99 of LpxK would serve to increase the pK_a of H261, allowing for deprotonation of the substrate and subsequent nucleophilic attack on the γ -phosphate of ATP (Scheme 2). The high optimal pH range for LpxK activity supports the inclusion of an activated histidine imidazole in the catalytic mechanism over a carboxylate functionality (Figure 1A), and the downshift in pK_a when the D99 carboxylate or H261 imidazole group is removed also lends credence to this assertion (Figure 5).

As a further endorsement of the hypothesis that the D99–H261 dyad is critical for LpxK activity, a significant kinetic distinction is made between the acidic residues of the Walker B motif (D138 and D139) and those of helix α 4 (D99 and E100) upon mutation (Table 2 and Figure 4A). Although alanine mutants of all these residues have reduced k_{cat} values (from 1000- to 8000-fold compared to that of wild-type LpxK), carboxamide mutants of D138 and D139 are more active than the corresponding alanine mutants, whereas the opposite is true for D99 and E100. This discrepancy reveals that side chain ionization of D99 and E100 must be required for efficient catalysis while it may not be necessary for D138 and D139. Because the carboxamide mutants retain some hydrogen bonding characteristics of the original carboxylates, D138 and D139 likely play a substrate positioning role because some activity is restored in the asparagine mutants when compared to alanine. D138, as stated previously, is thought to be involved in Mg^{2+} coordination, and D139 could be positioned to dock part of the DSMP substrate. The D139A mutation has a significant effect on the ATP/ Mg^{2+} K_m , indicating that its hydrogen bond to K51 could be involved in maintaining active site integrity (Table 2 and Figure 4A).

In the case of D99 and E100, the alanine mutants show reduced activity but may be somewhat compensated by an active site water molecule or nearby analogous side chain functionalities such as D260. The D99N and E100Q mutants cannot be ionized at physiological pH, and the bulky asparagine and glutamine residues block the compensatory functionalities from performing as well. As stated previously, D99 may be required to activate H261, increasing the pK_a of the distal nitrogen of the imidazole ring, so that the residue can in turn deprotonate the 4'-hydroxyl of DSMP (Scheme 2). The necessity of the E100 side chain to remain a carboxylate may be attributed to the fact that unlike D138, which is also predicted to coordinate the Mg^{2+} cation in the precatalytic state, E100 must remain bound to the cation throughout the catalytic process, thus making its charge state more critical to the overall mechanism.

CONCLUSION

Taken together, the additional crystal structures and kinetic characterization of LpxK have led to the proposal of a catalytic mechanism involving H261 as the primary catalytic base that, assisted by its interaction with D99, deprotonates the lipid substrate for nucleophilic attack. The closure of the C-terminal domain (Scheme 1) forms the active site catalytic dyad because D99 and H261 reside on the N- and C-terminal domains, respectively, and the crystal structure of ATP bound to the open conformation of LpxK likely highlights an intermediate step in this process. Other conserved residues in the LpxK

active site position the substrates for efficient transfer, not insignificant roles given the large perturbations in reaction velocity upon mutation for the majority of these side chains. Deciphering the catalytic roles of these residues is critical to inhibitor design and evaluation and improves the chances of successfully targeting this essential step in lipid A biosynthesis in the pursuit of novel antimicrobials. LpxK orthologs also represent a previously uncharacterized class of membrane-bound lipid kinases, and their study will further improve our understanding of common mechanisms and unique features of enzymatic catalysis at the membrane interface.

ASSOCIATED CONTENT

Supporting Information

Tables S1 and S2 describe the primers and strains used in this study. This material is available free of charge via the Internet at <http://pubs.acs.org>.

Accession Codes

The coordinates and structure factors for AMP-PCP–LpxK, ATP–LpxK, and compact P-loop–LpxK complexes have been deposited in the Protein Data Bank as entries 4ITL, 4ITM, and 4ITN, respectively.

AUTHOR INFORMATION

Corresponding Author

*R.P.E.: e-mail, ryan.emptage@duke.edu; phone, (919) 684-5178. P.Z.: e-mail, peizhou@biochem.duke.edu.

Funding

This work was supported by National Institutes of Health Grant GM-51310 (C.R.H.R. and P.Z.).

Notes

The authors declare no competing financial interest.

ACKNOWLEDGMENTS

Crystallization, screening, data collection, and data processing were performed at the Duke University X-ray Crystallography Shared Resource. Diffraction data were collected at the Southeast Regional Collaborative Access Team (SERCAT) 22-BM beamline at the Advanced Photon Source. Use of the APS was supported by the U.S. Department of Energy, Office of Science, and the Office of Basic Energy Sciences under Contract W-31-109-Eng-38. We also thank Dr. Anthony S. Serianni for providing methyl 2-acetamido-2-deoxy- β -D-glucopyranoside and Drs. Teresa Garrett, Kelly Daughtry, and Samuel Gattis for careful review of the manuscript. Finally, we thank the members of the Raetz lab for helpful discussion.

ABBREVIATIONS

AMP-PCP, 5'-adenylyl (β,γ -methylene)diphosphonate; bis-Tris, bis(2-hydroxymethyl)iminotris(hydroxymethyl)methane; CMC, critical micelle concentration; DDM, dodecyl maltoside; DSMP, tetraacyldisaccharide-1-phosphate; EDTA, ethylenediaminetetraacetic acid; HEPES, 4-(2-hydroxyethyl)-1-piperazineethanesulfonic acid; KDO, 3-deoxy-D-manno-oct-2-ulosonic acid; LPS, lipopolysaccharide; MPD, 2-methyl-2,4-pentanediol; NTP, nucleotide triphosphate; PDB, Protein Data Bank; P-loop, glycine-rich loop implicated in phosphate binding for enzymes that utilize NTPs; rmsd, root-mean-square deviation; SDS-PAGE, sodium dodecyl sulfate–polyacrylamide gel electrophoresis; TLC, thin-layer chromatography; Tris, 2-amino-2-(hydroxymethyl)-1,3-propanediol.

■ REFERENCES

- (1) Raetz, C. R. H., and Whitfield, C. (2002) Lipopolysaccharide endotoxins. *Annu. Rev. Biochem.* 71, 635–700.
- (2) Park, B. S., Song, D. H., Kim, H. M., Choi, B. S., Lee, H., and Lee, J. O. (2009) The structural basis of lipopolysaccharide recognition by the TLR4-MD-2 complex. *Nature* 458, 1191–1195.
- (3) Raetz, C. R. H., Reynolds, C. M., Trent, M. S., and Bishop, R. E. (2007) Lipid A modification systems in Gram-negative bacteria. *Annu. Rev. Biochem.* 76, 295–329.
- (4) Cheek, S., Zhang, H., and Grishin, N. V. (2002) Sequence and structure classification of kinases. *J. Biol. Chem.* 320, 855–881.
- (5) Ray, B. L., and Raetz, C. R. H. (1987) The biosynthesis of Gram-negative endotoxin. A novel kinase in *Escherichia coli* membranes that incorporates the 4'-phosphate of lipid A. *J. Biol. Chem.* 262, 1122–1128.
- (6) Garrett, T. A., Kadrmas, J. L., and Raetz, C. R. H. (1997) Identification of the gene encoding the *Escherichia coli* lipid A 4'-kinase. Facile phosphorylation of endotoxin analogs with recombinant LpxK. *J. Biol. Chem.* 272, 21855–21864.
- (7) Punta, M., Coggill, P. C., Eberhardt, R. Y., Mistry, J., Tate, J., Boursnell, C., Pang, N., Forslund, K., Ceric, G., Clements, J., Heger, A., Holm, L., Sonnhammer, E. L. L., Eddy, S. R., Bateman, A., and Finn, R. D. (2012) The Pfam protein families database. *Nucleic Acids Res.* 40, D290–D301.
- (8) Walker, J. E., Saraste, M., Runswick, M. J., and Gay, N. J. (1982) Distantly related sequences in the α - and β -subunits of ATP synthase, myosin, kinases and other ATP-requiring enzymes and a common nucleotide binding fold. *EMBO J.* 1, 945–951.
- (9) Emptage, R. P., Daughtry, K. D., Pemble, C. W., IV, and Raetz, C. R. H. (2012) Crystal structure of LpxK, the 4'-kinase of lipid A biosynthesis and atypical P-loop kinase functioning at the membrane interface. *Proc. Natl. Acad. Sci. U.S.A.* 109, 12956–12961.
- (10) Plötz, B. M., Lindner, B., Stetter, K. O., and Holst, O. (2000) Characterization of a novel lipid A containing D-galacturonic acid that replaces phosphate residues. The structure of the lipid A of the lipopolysaccharide from the hyperthermophilic bacterium *Aquifex pyrophilus*. *J. Biol. Chem.* 275, 11222–11228.
- (11) Mamat, U., Schmidt, H., Munoz, E., Lindner, B., Fukase, K., Hanuszkiewicz, A., Wu, J., Meredith, T. C., Woodard, R. W., Hilgenfeld, R., Mesters, J. R., and Holst, O. (2009) WaaA of the hyperthermophilic bacterium *Aquifex aeolicus* is a monofunctional 3-deoxy-D-manno-oct-2-ulosonic acid transferase involved in lipopolysaccharide biosynthesis. *J. Biol. Chem.* 284, 22248–22262.
- (12) Leipe, D. D., Koonin, E. V., and Aravind, L. (2003) Evolution and classification of P-loop kinases and related proteins. *J. Mol. Biol.* 333, 781–815.
- (13) Hutter, M. C., and Helms, V. (2000) Phosphoryl transfer by a concerted reaction mechanism in UMP/CMP-kinase. *Protein Sci.* 9, 2225–2231.
- (14) Charlier, H. A., Runquist, J. A., and Miziorko, H. M. (1994) Evidence supporting catalytic roles for aspartate residues in phosphoribulokinase. *Biochemistry* 33, 9343–9350.
- (15) Forstner, M., Muller, A., Stoltz, M., and Wallmann, T. (1997) The active site histidines of creatine kinase. A critical role of His 61 situated on a flexible loop. *Protein Sci.* 6, 331–339.
- (16) Negishi, M., Pedersen, L. G., Petrotchenko, E., Shevtsov, S., Gorokhov, A., Kakuta, Y., and Pedersen, L. C. (2001) Structure and function of sulfotransferases. *Arch. Biochem. Biophys.* 390, 149–157.
- (17) Miroux, B., and Walker, J. E. (1996) Over-production of proteins in *Escherichia coli*: Mutant hosts that allow synthesis of some membrane proteins and globular proteins at high levels. *J. Mol. Biol.* 260, 289–298.
- (18) Inoue, H., Nojima, H., and Okayama, H. (1990) High efficiency transformation of *Escherichia coli* with plasmids. *Gene* 96, 23–28.
- (19) McLerren, A. L., Zhou, P., Guan, Z., Raetz, C. R. H., and Rudolph, J. (2005) Kinetic analysis of the zinc-dependent deacetylase in the lipid A biosynthetic pathway. *Biochemistry* 44, 1106–1113.
- (20) Bartling, C. M., and Raetz, C. R. H. (2008) Steady-state kinetics and mechanism of LpxD, the N-acyltransferase of lipid A biosynthesis. *Biochemistry* 47, 5290–5302.
- (21) Otwinowski, Z., and Minor, W. (1997) Processing of X-ray diffraction data collected in oscillation mode. *Methods Enzymol.* 276, 307–326.
- (22) Adams, P. D., Afonine, P. V., Bunkóczki, G., Chen, V. B., Davis, I. W., Echols, N., Headd, J. J., Hung, L. W., Kapral, G. J., Gross-Kunstleve, R. W., McCoy, A. J., Moriarty, N. W., Oeffner, R., Read, R. J., Richardson, D. C., Richardson, J. S., Terwilliger, T. C., and Zwart, P. H. (2010) PHENIX: A comprehensive Python-based system for macromolecular structure solution. *Acta Crystallogr. D66*, 213–221.
- (23) Emsley, P., Lohkamp, B., Scott, W. G., and Cowtan, K. (2010) Features and development of Coot. *Acta Crystallogr. D66*, 486–501.
- (24) Chen, V. B., Arendall, W. B., III, Headd, J. J., Keedy, D. A., Immormino, R. M., Kapral, G. J., Murray, L. W., Richardson, J. S., and Richardson, D. C. (2010) MolProbity: All-atom structure validation for macromolecular crystallography. *Acta Crystallogr. D66*, 12–21.
- (25) DeLano, W. L., and Lam, J. W. (2005) PyMOL: A communications tool for computational models. *Abstracts of Papers of the American Chemical Society* 230, U1371–U1372.
- (26) Hu, X. S., Zhang, W. H., Oliver, A. G., and Serianni, A. S. (2011) Methyl 2-acetamido-2-deoxy- β -D-glucopyranoside dihydrate and methyl 2-formamido-2-deoxy- β -D-glucopyranoside. *Acta Crystallogr. C67*, o146–o150.
- (27) Carman, G. M., Deems, R. A., and Dennis, E. A. (1995) Lipid signaling enzymes and surface dilution kinetics. *J. Biol. Chem.* 270, 18711–18714.
- (28) Dodson, G., and Wlodawer, A. (1998) Catalytic triads and their relatives. *Trends Biochem. Sci.* 23, 347–352.
- (29) Garrett, T. A., Que, N. L., and Raetz, C. R. H. (1998) Accumulation of a lipid A precursor lacking the 4'-phosphate following inactivation of the *Escherichia coli lpxK* gene. *J. Biol. Chem.* 273, 12457–12465.
- (30) Krell, T., Maclean, J., Boam, D. J., Cooper, A., Resmini, M., Brocklehurst, K., Kelly, S. M., Price, N. C., Lapthorn, A. J., and Coggins, J. R. (2001) Biochemical and X-ray crystallographic studies on shikimate kinase: The important structural role of the P-loop lysine. *Protein Sci.* 10, 1137–1149.
- (31) Knowles, J. R. (1976) The intrinsic pK_a-values of functional groups in enzymes: Improper deductions from the pH-dependence of steady-state parameters. *Crit. Rev. Biochem.* 4, 165–173.
- (32) Adams, J. A. (2001) Kinetic and catalytic mechanisms of protein kinases. *Chem. Rev.* 101, 2271–2290.
- (33) Badola, P., and Sanders, C. R., II (1997) *Escherichia coli* diacylglycerol kinase is an evolutionarily optimized membrane enzyme and catalyzes direct phosphoryl transfer. *J. Biol. Chem.* 272, 24176–24182.
- (34) Belunis, C. J., and Raetz, C. R. H. (1992) Biosynthesis of endotoxins. Purification and catalytic properties of 3-deoxy-D-manno-octulosonic acid transferase from *Escherichia coli*. *J. Biol. Chem.* 267, 9988–9997.
- (35) Six, D. A., Carty, S. M., Guan, Z., and Raetz, C. R. H. (2008) Purification and mutagenesis of LpxL, the lauroyltransferase of *Escherichia coli* lipid A biosynthesis. *Biochemistry* 47, 8623–8637.